

DESIGN FOR ADDITIVE MANUFACTURING – MATERIAL CHARACTERIZATION AND GEOMETRICAL OPTIMIZATION

FRANCO CONCLI¹* & MARGHERITA MOLINARO²

¹Free University of Bolzano/Bozen, Faculty of Science and Technology, Bolzano, Italy.

²University of Udine, Polytechnic Department of Engineering and Architecture, Udine, Italy.

ABSTRACT

Additive manufacturing (AM) is a more and more appreciated manufacturing technology. This growing interest is related to the high flexibility of this approach and its capability to produce any geometry, opening new possibilities. An example is the improvement of the system performances exploiting lattice and reticular in substitution to the traditional solid design. Despite this premise, in real applications, part of the benefits is lost due to the inferior performances of the AM steels and the higher costs of additive manufacturing. In this scenario, the mechanical properties of a 17-4 PH SS produced via additive technology were characterized with experimental tests. The results were compared with data concerning the cast material. In this way, it was possible to execute a quantitative evaluation of the performance reduction. Three components, such as a hip prosthesis, a blow plastic bottle die, and an automotive gear, were chosen as representative examples. These three mechanical components are typically produced in quite different batch sizes. The hip prosthesis, the blow plastic bottle die, and the automotive gear were redesigned (design for AM) via a finite element (FE) approach. The new designs fulfill the original requirements in terms of strength showing however improved inertial properties. The original and new designs were exploited to quantify the benefits of introducing AM in different applications.

Keywords: additive manufacturing, finite elements, optimization.

1 INTRODUCTION

The objective of the present study is to determine the effectiveness of AM technology as an alternative to chip removal processes. The focus is on the (experimental) characterization of the mechanical properties of a 17-4 PH SS, both in the AM versions and its wrought counterpart.

Selective laser melting (SLM) was used to manufacture two series of samples whose geometry was chosen according to the ASTM-E606 [1] standard. A third series turned from a cast material via turning operations.

Some scholars have observed a slight increment in the mechanical properties of AM 17-4 PH SS with respect to the traditional counterpart [2]. This evidence could be justified considering the manufacturing process characteristics. The AM, in fact, promotes a higher cooling rate that leads to a different microstructure [3]. The higher solidification rate that characterizes the SLM process impedes the formation of martensite promoting instead an austenitic microstructure [4–6]. As far as the structural properties of the AM 17-4 PH SS are concerned, the opinions of scholars differ. Some of them pointed out that they could be negatively affected by the porosities resulting from the production process [7–10], which act as nucleation sites. Others have instead proven how the presence of surface defects induced by the AM process could promote better lubrication [11].

AM, thanks to its flexibility, can be used to produce any kind of topology allowing the exploitation of lightened structures such as lattices and reticular. These latter structures have typically very small dimensions and, under operation, local plastic deformations could often not be avoided [12–14].

With these premises, to include all these effects in the design of a new AM component, the deep knowledge of the quasi-static (QS) and the cyclic and the fatigue behavior are fundamental.

In this paper, the results of the experimental characterization of an AM 17–4 PH SS are presented in the form of Ramberg-Osgood (RO) curves, Basquin-Manson-Coffin (BMC) curves [15], and Wöhler curves [16, 17].

In addition to the test on the AM as-build samples, the effect of the surface finishing was studied using the second series of samples manufactured via SLM and successively grinded. The knowledge of the characteristics is of fundamental importance, especially since in the majority of applications the lattice/reticular are set into operations without additional finishing processes. Finally, experiments were also conducted on a series of 17–4 PH SS turned from a casted bar.

Based on the results of the material characterization campaign, a geometry optimization of three mechanical components was done exploiting finite elements (FE). The optimization focuses on the strut's diameter and the size of the elementary cell. The optimization was aimed at reducing the component mass. The optimized geometries fulfill the requirements of the original counterparts. The original and the new designs were compared to evaluate the benefits of using AM as a substitution to traditional manufacturing.

2 MATERIAL PROPERTIES

Figure 1 shows the sample geometries used for the quasi-static (QS) and the low cycle fatigue (LCF) tests. In both cases, the samples have a cylindrical shape. The active length is 10 mm for the QS samples and 4.28 mm for the LCF samples. The lengths differ: 5 mm for the QS geometry and 2 mm for the LCF geometry. The geometry was selected according to the ASTM E606 standard [1].

Table 1 summarizes the chemicals of the AM powder.

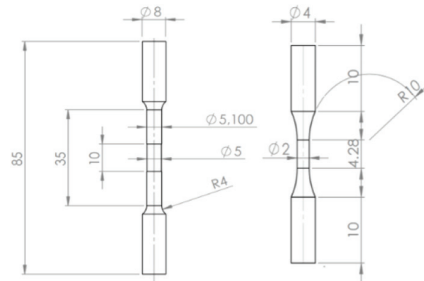


Figure 1: Sample geometries: (a) QS and (b) LCF tests.

Table 1: Chemical composition of powder 17-4 PH SS.

Carbon	Silicon	Manganese	Phosphorus	Sulfur	Chromium	Nickel	Molybdenum
0.0360	0.7800	0.3300	0.0090	0.0040	16.20	4.0200	0.0020

A. Quasi-static tests

At the Free University of Bolzano/Bozen, an electromechanical 5kN testing machine is available, namely, a STEPLab UD04 (Fig. 2).

The QS tests were performed on this apparatus and fixed using mechanical clamping devices. During the QS test, the crosshead velocity was set to 0.1 mm/min to avoid dynamic effects and local variation of the sample temperature. All broken samples (three repetitions) exhibit the cone-cup ductile fracture. The yielding for the AM 17-4 PH SS was quantified in 590 MPa, resulting below the one measured on the wrought 17-4 PH samples (980 MPa) [18–21] (Fig. 3). The measuring accuracy was about 2 N, i.e. about 0.1 MPa for the QS samples.

The LCF experiments were conducted under strain control on the STEPLAB UD04 tensile machine used for the QS characterization. The LCF tests were performed with a strain ratio $R_e = -1$. The frequency for the tests was chosen according to the minimum value prescribed by the standard ASTM E606 [1], 0.1 Hz. All the tests were continued up to the failure. After approximately 1/3 of the life, the hysteresis cycle resulted stable. These values were interpolated via the Ramberg–Osgood (RO) model (Fig. 4):

$$\varepsilon_a = \varepsilon_{ae} + \varepsilon_{ap} = \frac{\sigma_a}{E} + \left(\frac{\sigma_a}{K'} \right)^{\frac{1}{n'}} \quad (1)$$



Figure 2: SLM machine, STEPLAB UD04 tensile testing equipment, and details of the clamping device.

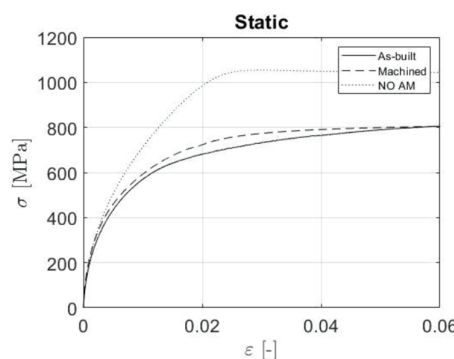


Figure 3: Results of the QS tests.

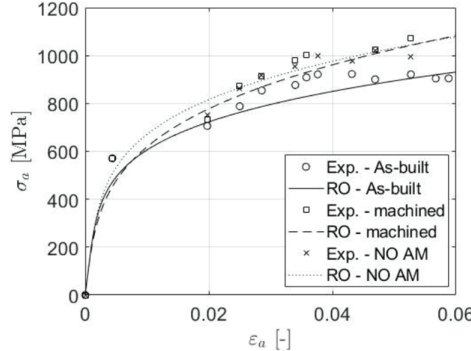


Figure 4: RO stress–strain curves [24, 25].

Table 2: Constants of the Ramberg–Osgood equation.

Sample	K' [GPa]	n' [-]	E [GPa]
As-built	1.705	0.20920	210
Machined	2.392	0.27300	210
NO AM	2.088	0.22760	2100

where ε_{ae} and ε_{ap} represent the elastic and plastic amplitudes of the strain, σ_a is the stress amplitude, E is the Young module, K' and n' are parameters [22]. Please be aware that, in the present form, K' and n' do not have the same meaning as the normally used Hollomon parameters [23].

The RO-tuned constants are shown in Table 2.

While the stable condition was exploited to tune the cyclic curve, the final failure of each sample (strain amplitude and the number of achieved cycles) is used to determine the coefficient of the Basquin–Manson–Coffin (BMC) equation.

$$\varepsilon_a = \frac{\Delta\varepsilon}{2} = \frac{\Delta\sigma'_f}{E} (2N)^b + \varepsilon'_f (2N)^c \quad (2)$$

The BMC equation consists of two parts. The first term $\frac{\Delta\sigma'_f}{E} (2N)^b$, called Basquin's term, refers to the elastic deformation. The second part of the equation is called Manson–Coffins term and describes the plastic strain. The Basquin parameters σ'_f and b are called the fatigue strength coefficient and the fatigue strength exponent, respectively. The Manson–Coffin parameters ε'_f and c are instead the fatigue ductility coefficient and the fatigue ductility exponent. These values were determined based on 10 LCF tests for each material, following the ASTM 739 procedure [26].

The determination of the Basquin coefficients (σ'_f and b) requires the knowledge of the yield stress σ_Y and the fatigue limit σ_F [27]. The Basquin term is used to break up the total deformation ε_a into its elastic ε_{ae} and plastic ε_{ap} parts.

$$\varepsilon_{ap} = \varepsilon_a - \varepsilon_{ae} = \varepsilon'_f (2N)^c \quad (3)$$

To estimate ε'_f and c , eqn 3 should be expressed as:

$$\log(N) = \hat{A} + \hat{B} \log(\varepsilon_{ap}) \quad (4)$$

A and B are the maximum likelihood (ML) estimators defined as:

$$\hat{A} = \bar{Y} - \hat{B}\bar{X} \quad (5)$$

$$\hat{B} = \frac{\sum(x_i - \bar{X})(y_i - \bar{Y})}{\sum_i} \quad (6)$$

\bar{X} and \bar{Y} are the averaged dependent variable $x_i (\log \varepsilon_{ap})$ and independent variable $y_i (\log N)$. The plastic strain amplitude (eqn 4) can be rewritten as:

$$\varepsilon_{ap} = 10^{\frac{-\hat{A}}{\hat{B}}} \left(\frac{1}{2} \right)^{\frac{1}{\hat{B}}} (2N)^{\frac{1}{\hat{B}}} \quad (7)$$

The ML estimators of the coefficients ε'_f and c (eqn 3) of the Manson–Coffin equation are calculated as:

$$\varepsilon'_f = 10^{\frac{-\hat{A}}{\hat{B}}} \left(\frac{1}{2} \right)^{\frac{1}{\hat{B}}} \text{ and } c = 1/\hat{B} \quad (8)$$

The parameters of the calibrated BMC curve are shown in Table 3.

From Fig. 5, it is possible to notice how the machined series of samples is better performing than the as-built one. The cast material (NO AM) shows the worst performance.

Table 3: Parameters of the Basquin–Manson–Coffin equation.

Sample	b	c	σ'_f	ε'_f
As-built	-0.02500	-0.23650	390.0	0.12630
Machined	-0.01600	-0.22040	426.0	0.12990
NO AM	-0.02200	-0.17120	489.0	0.08040

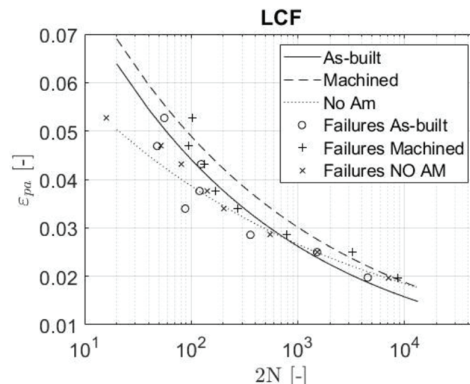


Figure 5: Resulting BMC curves.

3 REDESIGN FOR ADDITIVE MANUFACTURING

The flexibility of the additive manufacturing process [28] has opened up new possibilities promoting the optimization and redesign of components.

In the following chapter, the results of an optimization of three already existing components are summarized. As a benchmark, three components belonging to three completely different sectors were selected. Their shape was kept unaltered; the optimization process acted on the internal volume only. The optimization exploits the capability of AM to produce reticular/lattice structures in substitution to the traditional solid design leading to a significant reduction of the mass and the objects combined with material saving and a positive environmental impact.

The optimization procedure was applied to the elementary cells whose parameters were modified to fulfill the requirements in terms of resistance and stiffness. Three cell topologies, namely, the Body Centred Cubic, the Body Centred Cubic Z, and the Face Centred Cubic (Fig. 6) were selected as the most appropriate solutions for the optimization. A parametric archetypal of the elementary cell was modeled in the open-source environment Salome-Meca2020/Code_Aster [29]. The optimization was possible with the combination of the finite element (FE) software Code_Aster [30] and Dakota [31].

The optimization procedure started from the unitary loads that characterize the three components, such as hip prosthesis, blowing mold, and automotive gear.

After a preliminary simulation (for each component and cell topology combination), the diameter of the struts and the size of the elementary cell were modified. The following simulation was performed automatically. During the optimization procedure, two objective functions (mass minimization and stiffness maximization) were considered. The simulation parameters for the subsequent iterations were selected according to a MOGA approach (Pareto Front).

A. Hip prosthesis

Human movements are characterized by the biggest load variability. However, during walking, the loads lay in a direction that remains inside a small cone of action, in the superior zone of the acetabulum (Fig. 7).

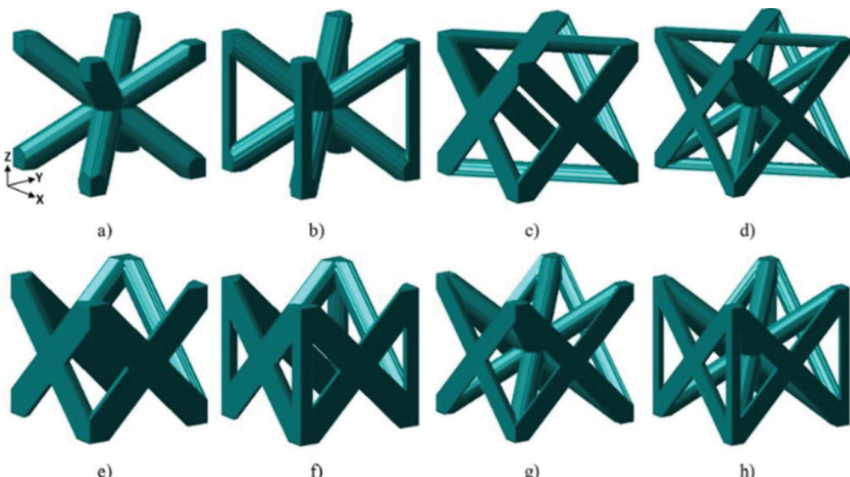


Figure 6: Cell topologies. For this study, the body-centered cubic (a), the body-centered cubic Z (b), and the face-centered cubic (c) were used.

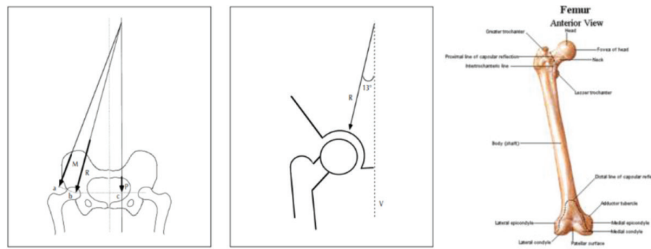


Figure 7: Loads on the hip prosthesis.

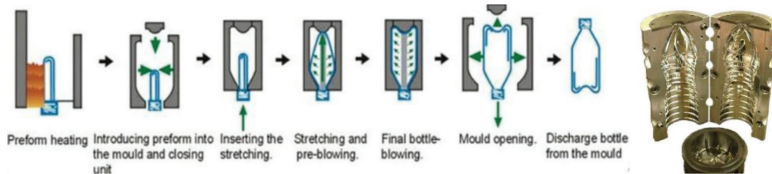


Figure 8: Blow molding process.

In case of monopodial loading, the force results in 7–10 times the body weight of a person. On these bases, the maximum load acting on the prosthesis was quantified in 6670N (person of 85 kg).

The contact area sandwiched between the femur head and the acetabulum cavity is around 0.003. This results in contact pressure of about 2.2 MPa. This value was used as a constraint for the optimization.

B. Bottle blowing mold

The next component is a mold to produce plastic bottles (Fig. 8).

The material used for bottles is usually polyethylene terephthalate (PET). The production process consists of blowing pressured air into the PET into the stretching (Fig. 8) to let the sides stretch until they stick to the die. The pressure is typically 3.6 MPa.

C. Automotive gear

The mechanical component representative of the series production is the fifth gear of the gearbox of an FCA GrandePunto gearbox (Fig. 9). Considering that the maximum torque that can be transmitted by the secondary shaft of the gearbox is equal to 378 Nm, the average shear stress in the gear rim can be estimated at about 7.0 MPa.

All the stress levels are below the fatigue limit of any commercial steel by one or two orders of magnitude and far below those of the 17-4 PH SS [32].

Overall, the three considered components exhibit huge margins of optimization.

4 RESULTS OF THE OPTIMIZATION

A. Hip prosthesis

The results of the optimization of the different cell types for the single-size batch component, such as the hip prosthesis, are summarized in Table 4 and depicted in Fig. 10.



Figure 9: Automotive gearbox of a FIAT Grande Punto.

Table 4: Optimized radii and cell sizes for hip prosthesis.

Cell Topology	Strut r [mm]	Cell size [mm]
BCC	0.900	3.00
BCCZ	0.970	3.80
FCC	0.870	3.00

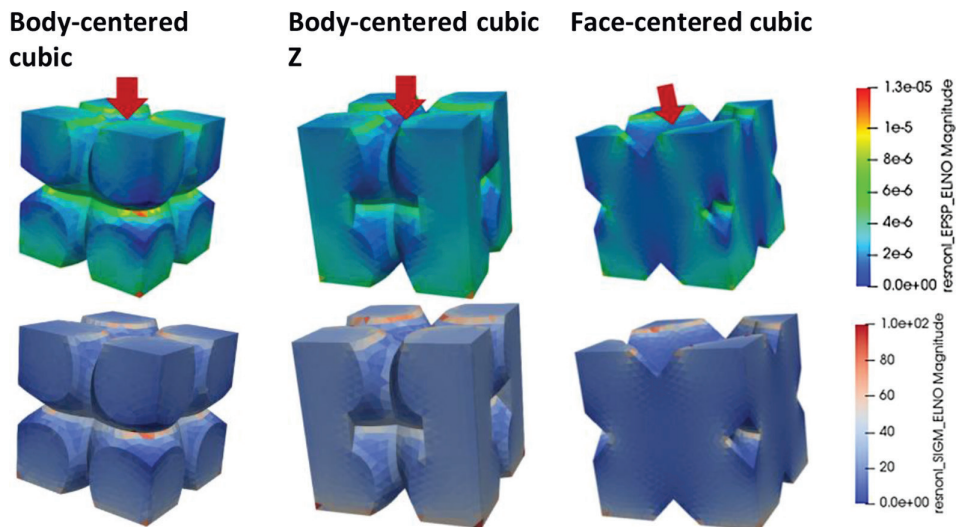


Figure 10: Optimization of the cells of the hip prosthesis.

B. Bottle blowing mold

The optimization of the three cell topologies for the die mold leads to the results shown in Table 5 and Fig. 11.

C. Automotive gear

The optimization lead, for what concerns the gear, to the following results (Table 6 and Fig. 12).

Table 5: Optimized radii and cell sizes for bottle blowing mold.

Cell topology	Strut r [mm]	Cell size [mm]
BCC	0.990	3.30
BCCZ	0.880	3.00
FCC	0.870	3.00

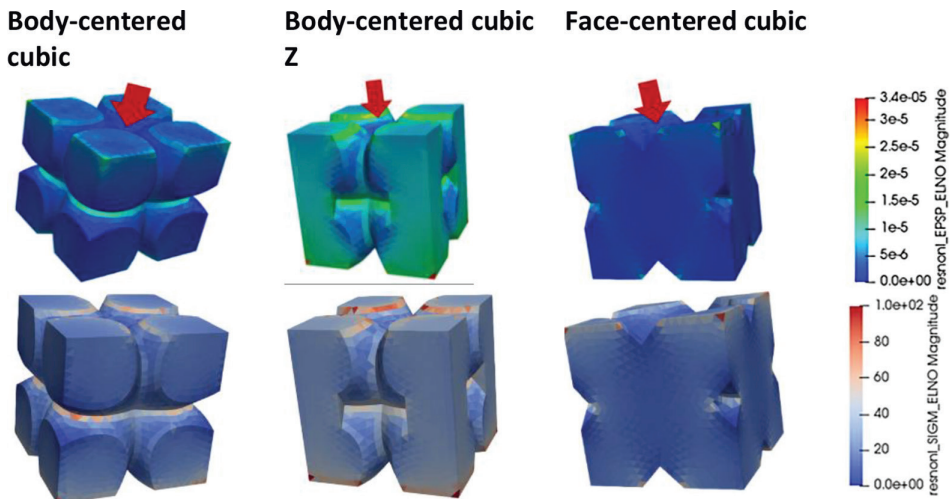


Figure 11: Optimization of the cells of the bottle blowing mold.

Table 6: Optimized radii and cell sizes for automotive gear.

Cell topology	Strut r [mm]	Cell size [mm]
BCC	0.900	3.30
BCCZ	0.880	3.20
FCC	0.800	3.00

5 DISCUSSION AND CONCLUSIONS

Through the coupling of an open-source FE software and the optimization tool DAKOTA, it was possible to analyze the impact of a redesign for AM on three components representative of different production batches [33–37]. Considering that AM relies primary on the possibility to substitute the solid design with lattice structures or reticula and that those architectures could not be grinded and should be set into operations in the as-built condition, a preliminary testing campaign was performed to collect reliable data on the impact of the surface roughness on the material performance. Considering that AM parts could not be grinded, the testing campaign was performed on the as-built and machine AM samples. Moreover, in order to have a direct comparison with traditional manufacturing, the third series of samples manufactured starting from cast material was tested.

The original design of the three analyzed components was optimized exploiting the reticula. The optimization was performed ensuring the same reliability and maximum deformation

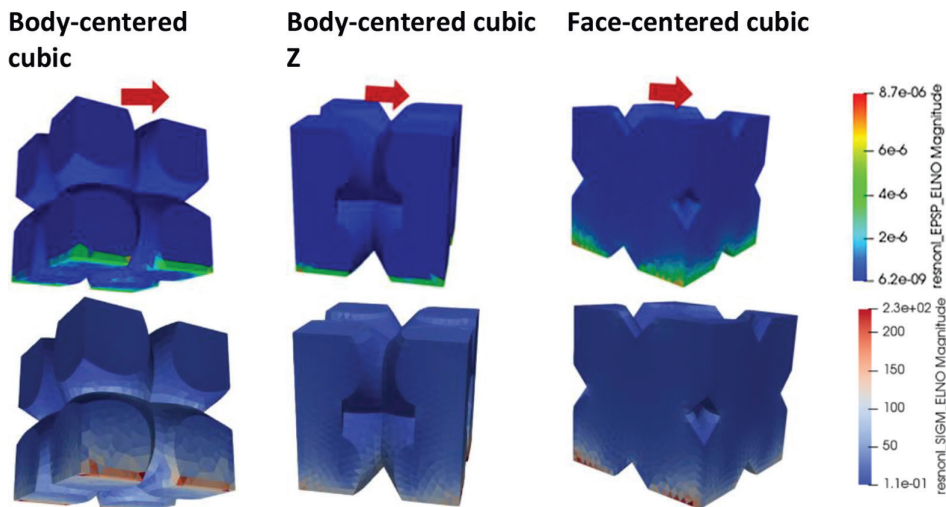


Figure 12: Optimization of the cells of the automotive gear.

of the original components. To achieve this goal, three reticular cell topologies such as BCC, BCCZ, and FCC were selected. Their strut diameters and cell size were changed based on FEM simulations combined with a multiobjective genetic algorithm.

A potential average weight reduction between 21% and 23% was obtained for each component.

NOMENCLATURE

AM	Additive manufacturing	HCF	High cycle fatigue
BCC	Body-centered cubic	LCF	Low cycle fatigue
BCCZ	Body-centered cubic-Z	RO	Ramberg–Osgood
BMC	Basquin–Manson–Coffin	SLM	Selective laser melting
FCC	Face-centered cubic	SS	Stainless steel
FE(M)	Finite element (method)		

FUNDING

The authors thank the FUB for the financial support given to this study through the projects M.AM.De (call CRC2017 Unibz PI Franco Concli, TM Margherita Molinaro) and APE (call RTD2021 Unibz PI Franco Concli, TM Margherita Molinaro).

REFERENCES

- [1] ASTM, .Standard test method for strain-controlled fatigue testing. *E606/E606M-12, 96(2004)*, pp. 1–16, 2004.
- [2] S. Cheruvathur, E. A. Lass, and C. E. Campbell, Additive manufacturing of 17-4 PH stainless steel: post-processing heat treatment to achieve uniform reproducible microstructure. *JOM*, **68**, pp. 930–942, 2016. <https://doi.org/10.1007/s11837-015-1754-4>
- [3] S. steel A. 17-4TM precipitation ATI technical data sheet and H. Alloy, Stainless steel AL 17-4™ precipitation hardening alloy. *Allegheny Technologies*, 2006.
- [4] C. N. Hsiao, C. S. Chiou, and J. R. Yang, Aging reactions in a 17-4 PH stainless steel. *Mater Chem Phys*, **74**(2), pp. 134–142, 2002. [https://doi.org/10.1016/S0254-0584\(01\)00460-6](https://doi.org/10.1016/S0254-0584(01)00460-6)

- [5] H. K. Rafi, D. Pal, N. Patil, T. L. Starr, and B. E. Stucker, Microstructure and mechanical behavior of 17-4 precipitation hardenable steel processed by selective laser melting. *J Mater Eng Perform*, **23**(12), pp. 4421–4428, 2014. <https://doi.org/10.1007/s11665-014-1226-y>
- [6] U. K. Viswanathan, S. Banerjee, and R. Krishnan, Effects of aging on the microstructure of 17-4 PH stainless steel. *Mater Sci Eng*, **104**(C), pp. 181–189, 1988. [https://doi.org/10.1016/0025-5416\(88\)90420-X](https://doi.org/10.1016/0025-5416(88)90420-X)
- [7] A. Yadollahi, N. Shamsaei, S. M. Thompson, A. Elwany, and L. Bian, Mechanical and microstructural properties of selective laser melted 17-4 ph stainless steel. *ASME International Mechanical Engineering Congress and Exposition, Proceedings (IMECE)*, **2A-2015**, 2015. <https://doi.org/10.1115/IMECE2015-52362>
- [8] J. H. Wu and C. K. Lin, Influence of high temperature exposure on the mechanical behavior and microstructure of 17-4 PH stainless steel. *J Mater Sci*, **38**(5), pp. 965–971, 2003. <https://doi.org/10.1023/A:1022377225704>
- [9] H. Mirzadeh and A. Najafizadeh, Aging kinetics of 17-4 PH stainless steel. *Mater Chem Phys*, **116**(1), pp. 119–124, 2009. <https://doi.org/10.1016/j.matchemphys.2009.02.049>
- [10] W. E. Luecke and J. A. Slotwinski, Mechanical properties of austenitic stainless steel made by additive manufacturing. *J Res Natl Inst Stand Technol*, **119**, pp. 398–418, 2014. <http://doi.org/10.6028/jres.119.015>
- [11] B. Lozanovski *et al.*, Computational modelling of strut defects in SLM manufactured lattice structures. *Mater Des*, **171**, 2019. <https://doi.org/10.1016/j.matdes.2019.107671>
- [12] X. Ren, J. Shen, P. Tran, T. D. Ngo, and Y. M. Xie, Design and characterisation of a tunable 3D buckling-induced auxetic metamaterial. *Mater Des*, **139**, pp. 336–342, 2018. <https://doi.org/10.1016/j.matdes.2017.11.025>
- [13] X. Ren, J. Shen, P. Tran, T. D. Ngo, and Y. M. Xie, Auxetic nail: design and experimental study. *Compos Struct*, **184**(2017), pp. 288–298, 2018. <https://doi.org/10.1016/j.compstruct.2017.10.013>
- [14] L. Yang, O. Harrysson, H. West, and D. Cormier, Correction to: modeling of uniaxial compression in a 3D periodic re-entrant lattice structure. (*Journal of Materials Science*, **48**(4), pp. 1413–1422, 2013. <https://doi.org/10.1007/s10853-012-6892-2>),” *J Mater Sci*, **55**(21), p. 9144, 2020.
- [15] M. Mahmoudi, A. Elwany, A. Yadollahi, S. M. Thompson, L. Bian, and N. Shamsaei, Mechanical properties and microstructural characterization of selective laser melted 17-4 PH stainless steel. *Rapid Prototyp J*, **23**(2), pp. 280–294. 2017. <https://doi.org/10.1108/RPJ-12-2015-0192>
- [16] T. Maconachie *et al.*, SLM lattice structures: properties, performance, applications and challenges. *Materials and Design*, **183**, 108137, 2019. <https://doi.org/10.1016/j.matdes.2019.108137>
- [17] P. Köhnen, C. Haase, J. Bültmann, S. Ziegler, J. H. Schleifenbaum, and W. Bleck, Mechanical properties and deformation behavior of additively manufactured lattice structures of stainless steel. *Mater Des*, **145**, pp. 205–217, 2018. <https://doi.org/10.1016/j.matdes.2018.02.062>
- [18] F. Concli, A. Gilioli, and F. Nalli, Experimental–numerical assessment of ductile failure of additive manufacturing selective laser melting reticular structures made of Al A357. *Proc Inst Mech Eng Part C J Mech Eng Sci*, **32**(7), pp. 3047–3056, 2019. <https://doi.org/10.1177/0954406219832333>
- [19] F. Nalli, L. Cortese, and F. Concli, Ductile damage assessment of Ti6Al4V, 17-4PH and AlSi10Mg for additive manufacturing. *Eng Fract Mech*, **241**, 2021. <https://doi.org/10.1016/j.engfracmech.2020.107395>

- [20] L. Bonaiti, F. Concli, C. Gorla, and F. Rosa, Bending fatigue behaviour of 17-4 PH gears produced via selective laser melting, *Procedia StructIntegr*, **24**, pp. 764–774, 2019. <https://doi.org/10.1016/j.prostr.2020.02.068>
- [21] F. Concli and A. Gilioli, Numerical and experimental assessment of the static behavior of 3D printed reticular Al structures produced by selective laser melting: progressive damage and failure. *Procedia Struct Integr*, **12**, pp. 204–212, 2018. <https://doi.org/10.1016/j.prostr.2018.11.094>
- [22] W. Ramberg and W. R. Osgood, *Description of stress-strain curves by three parameters*. Washington, DC, 1943.
- [23] J. R. Hollomon, Tensile deformation. *Trans. AIME*, **162**, pp. 268–277, 1945.
- [24] L. Maccioni, E. Rampazzo, F. Nalli, Y. Borgianni, and F. Concli, Low-cycle-fatigue properties of a 17-4 PH stainless steel manufactured via selective laser melting. *Material and Manufacturing Technology XI*, **877**, pp. 55–60, 2021. <https://doi.org/10.4028/www.scientific.net/KEM.877.55>
- [25] L. Maccioni, L. Fraccaroli, and F. Concli, High-cycle-fatigue characterization of an additive manufacturing 17-4 PH stainless steel. *Key Engineering Materials*, 2020. <https://doi.org/10.4028/www.scientific.net/KEM.877.49>
- [26] ASTM, “Standard practice for statistical analysis of linear or linearized stress-life (s-n) and strain-life (e-n) fatigue data. *E ASTM 739-91*, 2006.
- [27] L. Maccioni, L. Fraccaroli, Y. Borgianni, and F. Concli, High-cycle-fatigue characterization of an additive manufacturing 17-4 PH stainless steel. *11th International Conference on Materials and Manufacturing Technologies*, **2020**, p. MT013.
- [28] Z. Alomar and F. Concli, A review of the selective laser melting lattice structures and their numerical models. *Adv Eng Mater*, **22(12)**, 2020. <https://doi.org/10.1002/adem.202000611>
- [29] www.code-aster.org
- [30] A. Gilioli, et al., Numerical and experimental assessment of the mechanical properties of 3D printed 18-Ni300 steel trabecular structures produced by selective laser melting—a lean design approach. *Virtual Phys Prototyp*, pp. 267–276, 2019. <https://doi.org/10.1080/17452759.2019.1565596>
- [31] <https://dakota.sandia.gov/>
- [32] L. Fraccaroli, et al., High and low cycle fatigue properties of 17-4 PH Manufactured via Selective Laser Melting in as-built, machined and hipped conditions. *Progress in Additive Manufacturing*, **7**, pp. 99–109, 2021. <https://doi.org/10.1007/s40964-021-00217-y>
- [33] Rampazzo E. et al., Design for additive manufacturing: is it an effective alternative? Part 1 – Material characterization and geometrical optimization. *WIT Transaction in Engineering Sciences*, **130**, 2021. <https://doi.org/10.2495/CMEM210081>
- [34] M. Molinaro et al., Design for additive manufacturing: is it an effective alternative? Part 2 – cost evaluation. *WIT Transaction in Engineering Sciences*, **130**, 2021. <https://doi.org/10.2495/CMEM210091>
- [35] L. Bonaiti, et al., High and low-cycle-fatigue properties of 17-4 PH manufactured via selective laser melting in as-built, machined and hipped conditions. *Progress Additive Manufacturing*, **7**, pp. 99–109, 2021. <https://doi.org/10.1007/s40964-021-00217-y>
- [36] Gerosa R., et al., Bending fatigue behavior of 17-4 PH gears produced by additive manufacturing. *App Sci*, **11(7)**, 3019, 2021. <https://doi.org/10.3390/app11073019>
- [37] M. Molinaro et al., Design for additive manufacturing: is it an effective alternative? Part 1 – material characterization and geometrical optimization. *WIT Transaction in Engineering Sciences*, **130**, 2021. <https://doi.org/10.2495/CMEM210081>